

Evolutionary stage of the spectral variable BD +48°1220 = IRAS 05040+4820

V.G. Klochkova, E.L. Chentsov, N.S. Tavganskaya & V.E. Panchuk

Special Astrophysical Observatory RAS, Nizhnij Arkhyz, 369167 Russia

October 31, 2018

Abstract Based on high-resolution observations ($R = 60000$ and 75000), we have studied the optical spectral variability of the star BD+48° 1220, associated with the IR source IRAS 05040 + 4820. We have measured the equivalent widths of numerous absorption lines of neutral atoms and ions within the region 4500–6760 Å, as well as the corresponding radial velocities. We use model atmospheres method to determine the effective temperature $T_{eff} = 7900$ K, surface gravity $\log g = 0.0$, microturbulence velocity $\xi_t = 6.0$, and the abundances for 16 elements. The metallicity of BD+48° 1220 differs little from the solar one: $[\text{Fe}/\text{H}] = -0.10$ dex. The main peculiarities of the chemical content of the star are a large helium excess, derived from the HeI 5876 Å absorption, $[\text{He}/\text{H}] = +1.04$, and the oxygen excess, $[\text{O}/\text{Fe}] = +0.72$ dex. The carbon overabundance is small, $[\text{C}/\text{Fe}] = +0.09$ dex, and the ratio $[\text{C}/\text{O}] < 1$. We obtained an altered relation for the light-metal abundances: $[\text{Na}/\text{Fe}] = +0.87$ dex with $[\text{Mg}/\text{Fe}] = -0.31$ dex. The barium abundance is lowered, $[\text{Ba}/\text{Fe}] = -0.84$ dex. We concluded that the selective separation of elements onto dust grains of the envelope is probably efficient. The radial velocity of the star measured from photospheric absorption lines over three years of observations varies in the interval $V_r = -(7 \div 15)$ km/s. Time variable differential line shifts have been revealed. The entire set of available data (the luminosity $M_v \approx -5^m$, velocity $V_{lsr} = -20$ km/s, metallicity $[\text{Fe}/\text{H}] = -0.10$, and peculiarities of the optical spectrum and chemical composition) confirms the status of BD+48° 1220 as a massive post-AGB star with He- and O- excesses belonging to the disk population.

1. Introduction

The 6 m telescope of the Special Astrophysical Observatory (SAO) has been used for spectroscopy of highly luminous stars with large IR-excesses on the asymptotic giant branch (AGB) or in the post-AGB stage. These objects are a transition stage to becoming a planetary nebula (for this reason, they are called protoplanetary nebulae, or PPN). PPN have passed through a long evolution: hydrogen and helium burning both in the core and in layer sources, mixing and mass loss via stellar wind at the AGB stage. The current theory of the evolution of intermediate-mass stars (see, for example, [1]) gives grounds to expect altered elemental abundances in the surface layers of these evolved objects. Our program is mainly aimed at determining the fundamental parameters of stars that likely belong to this class,

identifying their evolutionary stage, and searching for evolutionary variations of their chemical compositions. In addition, we are searching for spectral variability, and also carry out detailed study of the velocity fields in their atmospheres and envelopes, for comparison with those in supergiants and hypergiants and to reveal possible binarity in these objects. The basic results obtained in the program are summarized in [2, 3]. Papers [4, 5], which initiate our study of the spectroscopy of bipolar nebulae and of the peculiar hypergiant IRC +10420, whose evolution status has become fairly firm only recently (in particular, owing to our results [6, 7]), are also of interest in this context. Here, we present the results for our spectral observations of the thus far poorly studied star BD +48°1220 (SAO 40039, LSV +48° 26)–the optical counterpart of the IR-source IRAS 05040+4820 (from now on – IRAS 05040). BD +48°1220 displays a double-peaked spectral energy distribution (SED): the IRAS catalog [8] suggests somewhat high IR fluxes $f_{12}=0.25$, $f_{25}=7.20$, $f_{60}=20.20$, $f_{100}=11.00$.

The evolutionary stage of BD +48°1220 remains unclear. The star is situated fairly close to the plane of the Galaxy ($b = 4^m8$, $l = 159^m8$), which may indicate that it is young and probably belongs to the disk population. The high luminosity of BD +48°1220 and its two-peaked SED, which indicates the presence of circumstellar matter ejected in the course of its previous evolution, make it a good candidate post-AGB star, and Fujii et al. [9] recently did, in fact, assign BD +48°1220 to this stage. Based on multi-color optical photometric observations for a sample of high-luminosity stars, Fujii et al. [9] obtained for BD +48°1220 $B = 10^m1$ and $V = 9^m65$, and determined its spectral type to be $Sp = A4Ia$.

Using the 6 m telescope in combination with an echelle spectrograph during several observing seasons, we have obtained the first high resolution optical spectra of BD +48°1220, and detected substantial variability of the H I and metallic line profiles [10]. Here, we present the results of a detailed spectral study of BD +48°1220 using model atmospheres and synthetic spectra methods, as well as a detailed analysis of the pattern of radial velocities in the atmosphere of the star and the circumstellar space. Section 2 briefly describes our methods and the reduction of the spectral data, the peculiarities of the spectrum of BD +48°1220, and our results for its fundamental parameters. In Section 3, we discuss our results and the evolutionary status of the star.

2. Observations, data reduction and analysis

2.1. Echelle spectroscopy with the 6 m telescope

The spectroscopy of BD +48°1220 was carried out with the 6 m telescope of the SAO. All the spectra were obtained at the Nasmyth focus with the NES echelle spectrograph [11] equipped with a 2048×2048 CCD. In combination with the image slicer [12], the NES spectrograph provides a spectral resolution of $R = 60000$. Table 1 presents the dates of the observations, the integration times, the recorded spectral interval and S/N ratio. The data were extracted from the two-dimension echelle spectra using the modified [13] ECHELLE procedure of the MIDAS package running under an OS Linux. Hints of cosmic rays were removed via median averaging of pairs of consecutive spectra. The wavelength scale was calibrated using spectra produced by a Th-Ar lamp. The subsequent reduction, including photometric and position measurements, was carried out with the DECH20 code [14]. For each spectrogram, the position zero point was determined via a standard calibration using the positions of ionospheric night-sky emission lines and telluric absorption lines observed

against the background of the object's spectrum. The accuracy of the velocity measurements in the spectra obtained with the NES spectrograph is better than 1 km/s for a single line.

2.2. Main peculiarities of the optical spectrum

Emission features. As was already noted [10], the optical spectrum of BD +48°1220 displays numerous emission components. The H α line demonstrates a complex two-component emission profile, which is time-variable, as can be seen from Fig. 1. Here, the horizontal and vertical axes plot radial velocity V_{\odot} and intensity I (note that the continuum level is specified to be 100). The core of the H β line profile is also distorted by variable emission features. Variable emission components are also observed in the SiII, FeI, and FeII metal lines. To illustrate this fact, Fig. 2 presents the behavior of the FeII (55) 5534 Å line for several dates. In the spectrum obtained on March 8, 2004, the emission at $V_r \approx -20$ km/s is also visible in the profiles of the FeII 40, 46 and 74 multiple lines.

For a star whose effective temperature is below 8000 K, the HeI 5876 Å neutral helium absorption line is unexpectedly strong; its equivalent width, $W_{\lambda}(5875)=75$ mÅ, is measured reliably in all available spectra. The absorption nature of the line indicates its photospheric origin, as is also confirmed by the fact that the radial velocity corresponding to the position of the line is consistent with the velocity obtained from other weak absorption features (see Table 1 in the Appendix).

Interstellar features and color excess. A detailed examination of the high-resolution spectra shows that the NaI double resonance D-lines in the spectrum of BD +48° 1220 display complex profiles with several absorption components. Figure 3 presents the D1-line profiles for various observing times. Here, we can distinguish components whose positions correspond to the following velocities: three components in the velocity interval $V_{\odot} = -20$ to -30 km/s and a strong and broad component around $V_{\odot} \approx -2$ km/s ($V_{lsr}=-8$ km/s). According to Münch [15], interstellar D2 NaI lines are observed in a direction close to the position of BD +48°1220, whose position corresponds to sets of velocities $V_{lsr} \approx -4$ to -11 and -24 to -33 km/s. In the CO-band survey of the Milky Way [16], at a longitude of $l=160^{\circ}$, two intervals of the interstellar gas velocities are in a good consistency with the data of Münch [15]: $V_{lsr}=-10$ to $+7$, and -17 to -30 km/s.

The spectrum of BD +48°1220 is particularly remarkable for its numerous absorption features identified with diffuse interstellar bands (DIBs). Table 2 presents a list of such features and their equivalent widths W_{λ} , and the heliocentric velocities corresponding to the positions of these features are given in Tabl. 1 in the Appendix. The average velocity V_{\odot} derived from the interstellar bands presented in Tabl. 3 is consistent with that determined from the main component of the D-lines, $V_{\odot} \approx -2$ km/s ($V_{lsr} = -8$ km/s), which confirms its interstellar origin (Fig. 4).

Previously [10] the absolute luminosity $M_v \approx -5^m$ (luminosity type Ib) was obtained for BD +48°1220, which corresponds to a distance of $d \approx 5$ kpc, taking into account interstellar absorption. Using the calibration of Herbig [17] for $W_{\lambda}(5780)-E(B-V)$, we obtain from the measured value $W_{\lambda}=227$ mÅ for the 5780 Å band the color excess $E(B-V) \approx 0.4^m$, which leads us to the interstellar absorption $A_v \approx 1.2$. This suggests that the color excess of BD +48°1220 is due to interstellar absorption. However, according to Neckel and Klare [18], the absorption in the disk of the Galaxy in the direction towards the object in longitude $l=160^{\circ}$ already increases to $A_v \geq 1^m$ at a distance of 1 kpc. Thus, the formal application of Herbig's calibration substantially decreases the distance to the object. In the case of a

star with an envelope, some of the color excess can be due to absorption in the circumstellar region; therefore, the distance estimated from the amount of absorption can prove to be incorrect.

In the context of the star’s color excess, it is of interest to consider the optical polarizations of 26 PPN candidates determined by Parthasarathy et al. [19], including BD +48°1220. According to these data, BD +48°1220 belongs to a very small subgroup of stars with high polarizations: within the entire *BVRI* range, the degree of polarization is $p > 3\%$. The available wideband polarimetric data do not provide a firm description of the behavior of the polarization with increasing wavelength, hindering identification of the polarization mechanism. However, the high degree of polarization, which substantially exceeds the interstellar value for a color excess $E(B - V) \approx 0.4$, suggests that the radiation is polarized in the circumstellar environment of the star. In addition, measurements made on different dates display variability of the polarization: for example, in *V*, it varies from $p=3.15\%$ to 3.61% . This variability also confirms the “stellar” origin of the polarization, which, as in some other PPNs (IRAS 04296+3429, IRAS 08005–2356 [20]), could be associated with the asphericity and dynamics of the circumstellar envelope.

2.3. Parameters of the stellar atmosphere

To determine the main model parameters of the atmosphere, such as the effective temperature and gravity, and also to calculate the chemical composition and synthetic spectra, we used the grid of model stellar atmospheres [21] calculated in a hydrostatic approximation assuming local thermodynamic equilibrium (LTE) for various metallicities. The most difficult problem in calculating the chemical composition of a star is always fixing its basic parameters – the effective temperature T_{eff} and gravity $\log g$. For objects with uncertain evolutionary statuses, and hence uncertain reddening, it is difficult to apply photometric data to determine the effective temperature. Profiles of the hydrogen Balmer lines are widely used to determine the parameters of A–stars. However, the profiles of these lines in the spectrum of BD +48°1220 are distorted by variable emission. Therefore, we determined T_{eff} of the star using our spectral data, from the condition that the abundance from neutral iron be independent of the excitation potential of the FeI lines used. The gravity was determined from the condition that the iron atoms be in ionization balance, and the microturbulence velocity ξ_t from the condition that the iron abundance be independent of the line intensities. An additional criterion for the reliability of the method is the absence of this dependence for other elements represented in the spectra by numerous lines (CrII, TiII). In addition, if ξ_t is determined confidently, no dependence of the individual abundances on the equivalent widths of the lines used for the calculations should be seen.

The typical accuracies of the model parameters (on average) for a star with an effective temperature of about 8000 are $\Delta T_{eff} \approx 200$ K, $\Delta \log g \approx 0.5$ dex, $\Delta \xi_t \approx 0.5$ km/s. The high luminosity of BD +48°1220 is also confirmed by the very large equivalent widths of the ionized silicon SiII 6347, 6371Å lines: $W_\lambda=516$ and 490 mÅ, respectively (Fig. 5). According to Venn [22], the equivalent widths of the SiII 6347 Å lines in the spectra of stars in a sample of A0–F0 supergiants are a factor of 1.5–2 lower than in the spectrum of BD +48°1220. The application of a static plane-parallel model assuming LTE–approach to the unstable atmosphere of an A–supergiant may seem doubtful. This problem is considered in detail by Venn in [22]; however, Venn concluded here that blanketed Kurucz LTE models provide the best available fits for high luminous A–stars. Checking for a good correlation between the observed and synthetic

spectra provides a self-consistency test for obtained parameters. To check the reliability of the model atmosphere parameters, we compared the observed spectrum with a synthetic spectrum with the solar chemical composition and the model parameters $T_{eff}=7900$ K, $\log g=0.5$, and $\xi_t=6.0$ km/s calculated using the code [21]. This comparison (Fig. 5) shows reasonable consistency, with the exception of the strong SiIII lines. Table 4 presents the results of calculations of the chemical composition with the model $T_{eff}=7900$ K, $\log g=0.0$, $\xi_t=6.0$ km/s. The elemental abundances (X) calculated for individual lines with the parameters $T_{eff}=7900$ K, $\log g=0.5$, $\xi_t=6.0$ km/s are given in Table 2 in the Appendix, together with the oscillator strengths $\log gf$ and other atomic constants from the VALD database [24, 25]. Note that this table contains only the selected spectral lines used to derive the model parameters and elemental abundances.

3. Discussion of the results

3.1. Kinematics of the stellar atmosphere

All our measurements of the radial velocity V_{\odot} for various observing moments are presented in Tabl. 3, which shows that all the spectral features display time variability in V_{\odot} . For the period of our observations, the minimum variations in V_{\odot} were obtained for weak ($r \rightarrow 1$) absorption lines of metals: $V_{\odot}=-7$ to -15 km/s. The velocities derived from individual lines are given in Table 1 in the Appendix. Figure 4 presents the distribution of the radial velocities V_{\odot} measured from lines with different depths for one of the spectra (January 10, 2004). Here, the vertical and horizontal axes plot radial velocity and line depth (for the strongest lines, the depths on this scale are close to 100).

The systemic velocity V_{sys} is a fundamental parameter in the kinematic pattern shown by the lines of a star. But observations of BD +48°1220 at radio wavelengths [26, 27] have not revealed any spectral features that can be used to fix the value of V_{sys} . Therefore, as a first approximation, we adopted the average of the velocities for most weak absorption features: $V_{sys} \approx -13$ km/s ($V_{lsr} \approx -20$ km/s). This value is consistent with the velocities of HII regions in the local volume of the Galaxy in the direction towards BD +48°1220: $V_{lsr}(\text{HII}) \approx -20$ km/s [28]. Brand and Blitz [29] found the velocity $V_{lsr}(\text{HII}) \approx -20.5$ km/s in the same direction, for a distant region of the Galaxy at a distance of $d=5.2$ kpc. Recall that, according to our estimate (see Section 2.2), the distance to the star is $d \approx 5$ kpc. The absorption core of the $\text{H}\beta$ in the spectrum of BD +48°1220 is free of emission, and the velocity derived from the $\text{H}\beta$ core for two dates when it is detected is consistent with the value derived from the weak absorptions. The cores of the absorption lines of ions (FeII, CrII, etc.) indicate larger variations. The maximum displacement relative to weak lines was detected for the core of the $\text{H}\alpha$ line: at two epochs, this line is displaced short-ward of the systemic velocity by more than 10 km/s (Fig. 4). As follows from Fig. 4, the velocity corresponding to the position of the $\text{H}\alpha$ absorption is consistent with the position derived from the short-wavelength component of the NaI D-line, $V_{\odot} \approx -28$ km/s. Thus, in addition to the interstellar constituent, the short-wavelength component of D-lines NaI may also have a circumstellar (wind) contribution. Regrettably, the obtained spectra are insufficient for us to draw more definite conclusions. Obviously, further spectral monitoring and spectropolarimetry of the star are needed.

3.2. Chemical abundances pattern

Table 4 presents the adopted model atmosphere parameters T_{eff} , $\log g$, ξ_t and the average elemental abundances relative to iron, $[X/Fe]$. The chemical composition of the solar photosphere, relative to which we will consider the abundances in BD +48°1220, is taken from [23]. All the calculations of the chemical composition were made using codes developed by Shulyak et al. [21] and adapted for a PC running with OS Linux. The plane parallel LTE-models were calculated using the codes described in [21]. Corrections for hyperfine structure and isotopic shifts for the NiI, MnI, and BaII lines were not taken into account. The scatter of the abundances obtained from the set of lines is small: the *rms* deviation essentially does not exceed 0.3 dex (see Table 4). When determining the model parameters, we used lines with small and medium intensities with $W_\lambda \leq 0.25 \text{ \AA}$, since the approximation of a stationary plane-parallel atmosphere could be inadequate for the strongest spectral features. In addition, some strong absorption lines could be distorted by the effect of the circumstellar envelope; with insufficient spectral resolution, the intensity of envelope components is added to that of lines formed in the atmosphere.

The abundances were calculated for an extended set of lines: for some elements (MgI, TiII, CrII, FeII), we included lines with equivalent widths exceeding the above limit. As follows from Table 2 in the Appendix the abundances determined from strong lines do not differ systematically from those derived from lines with low and medium intensities. This is illustrated well by the results for silicon: the abundances derived from the weak SiII 4621 Å line and from two very strong SiII 6347 and 6371 Å lines coincide. Let us consider the detailed abundances, combining them into groups according to the type of elemental synthesis.

Light elements. As should be expected for a high-luminosity star, the abundances of some light elements are altered from their initial values. First and foremost, the helium excess derived from the HeI 5876 Å line stands out. Figure 6 compares the observed spectrum (for March 8, 2004) and the synthetic spectrum calculated for the model $T_{eff}=7900 \text{ K}$, $\log g=0.5$, $\xi_t=6.0 \text{ km/s}$ and the chemical composition from Table 4. The two spectra are in reasonable agreement.

Since the observed LiI 6707 Å line is very weak, the derived lithium excess is subject to considerable uncertainty.

We find an appreciable oxygen excess $[O/Fe]=+0.72$, with an almost normal carbon abundance $[C/Fe]=+0.09$; the ratio $C/O < 1$. Figure 7 compares the observed spectrum (January 10, 2004) with the synthetic spectrum. The essential oxygen excess indicates that BD +48°1220 cannot be a massive supergiant. Analyses of spectra of massive stars [30] shows that, in accordance with theoretical predictions, the evolution of a massive star leads to a deficit of oxygen, which is reprocessed into nitrogen in the course of the CNO cycle. Unfortunately, the detected spectral interval was limited to $\lambda=6760 \text{ \AA}$; therefore, no nitrogen lines were measured, although the N abundance is essential for determining the evolution stage of the star.

As we can see from Table 2 in the Appendix, the sodium abundance was determined from the weak NaI 5682, 5688, and 6160 Å lines, for which corrections due to deviations from LTE [31, 32] are the smallest. Therefore, the derived sodium excess, denotes the dispersion of the abundance obtained for a given number of lines n . The elemental abundances for the solar photosphere are taken from [23]. Sodium excess, $[NaI/Fe]=+0.87$, could basically be the result of sodium synthesis in the NeNa cycle, which occurs simultaneously with hydrogen burning in the CNO cycle [33, 34].

Iron-peak elements. The iron abundance, generally taken to be the metallicity, in the atmosphere of BD +48°1220 differs little from the solar value: $\log \varepsilon(\text{FeI}, \text{FeII})=7.37$. Sufficiently trustworthy abundances estimates for vanadium and chromium, which belong to the iron group, also display only small deviations from the normal values: $[\text{VII}, \text{CrI}, \text{CrII}/\text{Fe}]=+0.10$. A metallicity close to the solar value is consistent with the system's heliocentric radial velocity $V_{\odot} \approx -13 \text{ km/s}$, adopted in [10], which is typical for stars in the Galactic disk. However, the manganese, and especially nickel, abundances deviate substantially from the normal values. While the anomalous manganese abundance could be explained by our lack of inclusion of hyperfine structure of the lines and relatively low accuracy due to the small number of lines, the nickel overabundance $[\text{NiI}/\text{Fe}]=+0.74$ has been firmly determined from three medium intensity lines. Therefore, the nickel excess appears to be real.

Heavy metals. The large barium deficit relative to iron, $[\text{Ba}/\text{Fe}]=-0.84$, is typical of the atmospheres of supergiants. A deficiency of *s*-process elements in the atmospheres post-AGB stars is observed much more often than an excess [2, 35]. The observed lack of observed manifestations of the dredge-up of heavy metals is probably real, rather than resulting from systematic errors in the analysis of spectra of supergiants using model atmospheres. The presence or absence of *s*-process elements overabundance is probably related to the initial mass of the star and the mass-loss rate in the AGB stage, which specify the evolution of a given star and the mass of its core. Modelling of the process of third dredge-up [36] indicates that the efficiency of the dredge-up increases with the growth of the core mass (and hence of the initial mass) of a post-AGB star. Calculations made by Herwig [37] also show that the efficiency of the dredge-up increases if penetrating convection (overshooting) at the base of the convective zone is taken into account.

3.3. The separation of elements in the envelope

It is known that the selective separation of elements can provide an efficient mechanism for creating anomalous abundances of elements in atmospheres of stars with gas-dust envelopes. The star studied can undergo a stage of intense mass exchange between the atmosphere and the circumstellar gas-dust envelope; generally, the pattern of abundances is consistent with the dependence on the condensation temperature. Another argument in favor of separation is the enhanced zinc abundance: $[\text{Zn}/\text{Fe}]=+0.44$. The zinc abundance is a good test, since it is only slightly susceptible to selective condensation and does not vary in the course of the nuclear evolution of the given star. As was shown by Sneden et al. [38], within a large interval of metallicity, the zinc abundance corresponds to the behavior of iron, $[\text{Zn}/\text{Met}]=+0.04$. This conclusion was clarified by the recent results of Mishenina et al. [39], which showed that zinc followed the metallicity within the total studied interval $[\text{Fe}/\text{H}]=-0.5$ to -3.04 . For stars of the disk population, a slight increase of the zinc abundance with decreasing metallicity from $[\text{Fe}/\text{H}]=0$ to $[\text{Fe}/\text{H}]=-0.6$ dex has been obtained [40].

Additionally, we expect that elements with similar condensation temperatures T_{cond} should behave in the same way. For example, according to [23], T_{cond} for Ca and Sc are close. Indeed, as we can see from Table 4, these elements have very similar relative abundances in BD +48°1220. We conclude that the anomalous chemical composition can be explained by the selective condensation of atoms on dust grains in the circumstellar environs of the star. However, the fact that the iron abundance is close to the solar value indicates that anomalies of the elemental abundances introduced by condensation on dust grains are not very substantial, since iron is efficiently depleted onto dust grains. In addition, the behavior

of some elements is inconsistent with the dependence on the condensation temperature: for example, Ni, whose T_{cond} is close to that of Fe and V, displays an appreciable excess abundance. The situation is even more complicated by the fact that, apart from being affected by selective condensation, the abundances of some elements (C, O, Ba), can also vary due to nuclear processes in the course of the evolution of the star.

Chemical compositions similar to that obtained for BD +48°1220 are not unique for post-AGB stars. The elemental abundances in the atmospheres of PPNs can vary greatly (see, for example, the summaries in [2, 35]). Previously studied PPN candidates include stars with similarly anomalous chemical compositions. For example, HD 331319 (the optical counterpart of IRAS 19475+3119) also displays a metallicity close to the solar value, an excess of He, O, and light metals (Na, Si), and a deficit of Ti and Ba [42]. As in the case of BD +48°1220, the neutral He 5876 Å absorption is also observed ($W_\lambda=38$ mÅ in the spectrum of the F-supergiant HD 331319. Klochkova et al. [42] concluded that the He-lines were photospheric origin, and hence the He-excess due to the dredge-up of nuclear products synthesized during the evolution of the star was real. HD 161796 [42, 43] (the optical counterpart of IRAS 17436+5003) is another similar star. The A-supergiant HD 133656 (IRAS 15039–4806) [44] also displays a similar chemical abundances pattern; however, due to its decreased metallicity ($[Fe/H] \leq -0.7$), this star is assigned to an older population of the Galaxy.

3.4. Evolutionary status

Determining the evolutionary status of A-supergiants in the Galactic field is a nontrivial problem, since stars with substantially different ages and masses observed at very different evolutionary stages can display the same fundamental parameters, T_{eff} and $\log g$. The same region in the HR-diagram is occupied by post-AGB stars that are evolving from the AGB stage to planetary nebulae and young, massive supergiants evolving from the main sequence to the red supergiant stage. This problem of “spectral mimicry” is especially challenging, for example, for objects such as the peculiar hypergiant IRC+10420 [6, 7]. For BD +48°1220, the problem becomes even more complicated due to the fact that this supergiant is situated close to the Galactic plane, and the radial velocity pattern characteristic of supergiants is superimposed with differential shifts. According to the empirical chronological sequence [45], the absence of the standard features inherent to PPNs (maser lines of OH, H₂O, CO, etc.) in the radio spectrum of BD +48°1220 provides evidence that the star is close to the planetary nebula phase, as is confirmed by its fairly high effective temperature.

It is obvious that, when considering the evolutionary status of a star, the peculiarities of its chemical composition are critical. In the HR-diagram [46], the absolute magnitude $M_v \approx -5^m$ and $T_{eff}=7900$ K obtained for BD +48°1220 imply a fairly high mass for the star: $\mathcal{M} \approx 4M_\odot$. This value suggests that hot bottom burning (HBB) may be efficient [1], as is common for more massive AGB stars (the mass limit $\mathcal{M} \geq 4M_\odot$ depends on the metallicity). The possibility of efficient HBB is also supported by the peculiarities of the chemical composition of BD +48°1220, first and foremost, the lithium excess $[Li/Fe]=+0.62$. Unfortunately, due to the weakness of the LiI line, this excess has been determined with large uncertainty. However, the O-excess, the low C/O value, and the Na-excess in the atmosphere of BD +48°1220 are determined confidently, and support the efficiency of the HBB mechanism. The nitrogen abundance could be critical for verifying this hypothesis, making spectroscopy at longer wavelengths important.

4. Conclusions

Based on our observations with high spectral resolution ($R=60000$ and 75000), we have studied the optical spectrum of the A-supergiant BD +48°1220, the optical counterpart of the IR-source IRAS 05040+4820, in detail. At wavelengths from 4500 to 6760 Å, numerous absorption lines of neutral atoms and ions have been identified, and their equivalent widths and corresponding radial velocities have been measured. Using model atmospheres, we have obtained the effective temperature ($T_{eff}=7900$ K), gravity ($\log g=0.0$), microturbulence velocity ($\xi_t=6.0$), and the abundances of 16 chemical elements. The star displays close to solar metallicity: $[Fe/H]=-0.10$ dex. The abundances of the iron-group elements V and Cr display equally small deviations from their normal values: $[VII,CrI,ICrI/Fe]=+0.10$. The main feature of the chemical composition of the star is the large He-excess derived from the HeI 5876 Å line, $[He/H]=+1.04$, and the substantial O-excess $[O/Fe]=+0.72$ dex. The carbon excess is small: $[C/Fe]=+0.10$ dex. The relations between the abundances of light metals are anomalous: $[Na/Fe]=+0.87$ dex for $[Mg/Fe]=-0.31$ dex, while $[Na/Mg]=+1.18$ dex. The Ba abundance is appreciably low: $[Ba/Fe]=-0.84$ dex. The luminosity of the star and the peculiarities of its chemical composition (the excess of He, Li, and O with $[C/O]<1$) suggest that BD +48°1220 is related to more massive post-AGB stars, in which nuclear reactions occur at the base of the hot convective envelope in the AGB stage (hot bottom burning). In addition, some anomalies in the elemental abundances could be due to selective condensation onto dust grains of the envelope. This hypothesis is supported by the enhanced Zn abundance $[Zn/Fe]=+0.44$ and the similar deficits of Ca and Sc.

During the three years of our observations, the radial velocity of the star derived from photospheric absorptions varied in the interval $V_{\odot}=-7$ to -15 km/s. The available data ($M_v \approx -5^m$, $V_{lsr} \approx -20$ km/s, $[Fe/H]=-0.10$, the peculiarities of the optical spectrum and chemical composition) confirm the status of BD +48°1220 as a helium and oxygen-rich post-AGB star situated in the disk of the Galaxy.

Acknowledgements

This work was supported by the Russian Foundation for Basic Research (project code 05-07-90087), the program of basic research held by the Presidium of RAS “The origin and evolution of stars and the Galaxy”, program held by the Section for Physical sciences of RAS “Extended objects in the Universe”. This publication is based on work supported by Award No.RUP1-2687-NA-05 of the U.S. Civilian Research & Development Foundation (CRDF). In our study we used SIMBAD, ADS and VALD databases.

References

1. F.Herwig. *Ann. Rev. Astron. & Astrophys.*, **43**, 435, 2005.
2. V.G. Klochkova. *Bull. Spec. Astrophys. Obs.*, **44**, 5, 1998.
3. V.G. Klochkova, V.E. Panchuk, and R. Szczerba. *Astrophys. & Space Sci.*, **265**, 265, 2001.
4. V.G. Klochkova, V.E. Panchuk, M.V. Yushkin, and A.S. Miroshnichenko, *Astron. Report.*, **48**, 288, 2004.
5. V.G. Klochkova and E.L. Chentsov. *Astron. Report.*, **48**, 301, 2004.
6. V.G. Klochkova, E.L. Chentsov, and V.E. Panchuk. *MNRAS*, **292**, 19, 1997.
7. V.G. Klochkova, E.L. Chentsov, M. V. Yushkin, and V.E. Panchuk. *Astron. Report*, **46**, 139, 2002.
8. IRAS Catalogs, 1988. The point source catalog, version 2.0, NASA RP-1190 (NASA, Joint IRAS Working Group, 1988).
9. T. Fujii, Y. Nakada, and M. Parthasarathy, *Astron. & Astrophys.*, **385**, 884, 2002.
10. V.G. Klochkova, E.L. Chentsov, V.E. Panchuk, and M.V. Yushkin. *IBVS*, No.5584, 2004.
11. V.E. Panchuk, N.E. Piskunov, V.G. Klochkova, et al., *Preprint Spec. Astrophys. Observ.*, No.169, 2002.
12. V.E. Panchuk, M.V. Yushkin, and I.D. Naidenov, *Preprint Spec. Astrophys. Observ.*, No.179, 2003.
13. M.V. Yushkin and V.G. Klochkova. *Preprint Spec. Astrophys. Observ.*, No.206, 2005.
14. G.A. Galazutdinov. *Preprint Spec. Astrophys. Observ.*, No.102, 1992.
15. G. Münch. *Astrophys. J.*, **125**, 42, 1957.
16. T.M. Dame, D. Hartmann, and P. Thaddeus. *Astrophys. J.*, **547**, 792 (2001).
17. G. H. Herbi., *Astrophys. J.*, **407**, 142 (1993).
18. Th. Neckel, G. Klare, and M. Sarkander. *Astron. Astrophys. Suppl. Ser.*, **42**, 251 (1980).
19. M. Parthasarathy, S.K. Jain, and G. Sarkar. *Astron. J.*, **129**, 2451 (2005).
20. S.R. Trammell, H.L. Dinerstein, and R.W. Goodrich. *Astron. J.*, **108**, 984 (1994).
21. D. Shulyak, V. Tsymbal, T. Ryabchikova, et al. *Astron. & Astrophys.*, **428**, 993 (2004).
22. K. Venn. *Astrophys. J. Suppl. Ser.*, **99**, 659 (1995).
23. K. Lodders. *Astrophys. J.*, **591**, 1220 (2003).
24. N. E. Piskunov, F. Kupka, T. A. Ryabchikova, et al. *Astron. & Astrophys. Suppl. Ser.*, **112**, 525 (1995).
25. F. Kupka, N. E. Piskunov, T. A. Ryabchikova, et al. *Astron. Astrophys. Suppl. Ser.*, **138**, 119 (1999).

26. J.G.A. Wouterloot and J. Brand. *Astron. & Astrophys. Suppl. Ser.*, **80**, 149, 1989.
27. J.G.A. Wouterloot, J. Brand, and K. Fiegle. *Astron. Astrophys. Suppl. Ser.*, **98**, 589, 1993.
28. Y.P. Georgelin and Y.M. Georgelin. *Astron. & Astrophys.*, **6**, 349, 1970.
29. J. Brand and L. Blitz. *Astron. & Astrophys.*, **275**, 67, 1993.
30. K. Venn. *Astrophys. J.*, **414**, 316 (1993).
31. Y. Takeda and M. Takada–Hidai. *Publ. Astron. Soc. Japan*, **46**, 395, 1994.
32. Y. Takeda, G. Zhao, M. Takada–Hidai, et al. *Chinese J. Astron. & Astrophys.*, **3**, 316, 2003.
33. P.A. Denissenkov, V.V. Ivanov. *Astron. Lett.*, **13**, 214, 1987.
34. P.A. Denissenkov. *Astron. Lett.*, **14**, 435, 1989.
35. H. Van Winckel. *Astron. & Astrophys. Rev.*, **41**, 391, 2003.
36. F. Herwig and S.M. Austin. *Astrophys. J.*, **613**, L73, 2004.
37. F. Herwig. *Astron. & Astrophys.*, **360**, 952, 2000.
38. C. Sneden, R.G. Cratton, D.A. Crocker. *Astron. & Astrophys.*, **246**, 354, 1991.
39. T.V. Mishenina, V.V. Kovtyukh, C. Soubiran, et al. *Astron. & Astrophys.*, **396**, 189, 2002.
40. Y.-Q. Chen, P.E. Nissen, G. Zhao, *Astron. & Astrophys.*, **425**, 697, 2004.
41. G. Stasinska, R. Szczerba, M. Schmidt, and N. Siodmiak. *Astron. & Astrophys.*, **450**, 701, 2006.
42. V.G. Klochkova, V.E. Panchuk, N.S. Tavgaskaya. *Astron. Lett.*, **28**, 49, 2002.
43. R.E. Luck, H.E. Bond, D.L. Lambert. *Astrophys. J.*, **357**, 188, 1990.
44. H. Van Winckel, R.D. Oudmaijer, N.R. Trams. *Astron. & Astrophys.*, **312**, 553, 1996.
45. B.M. Lewis. *Astrophys. J.*, **338**, 234, 1989.
46. T. Blöcker. *Astron. & Astrophys.*, **299**, 755, 1995.

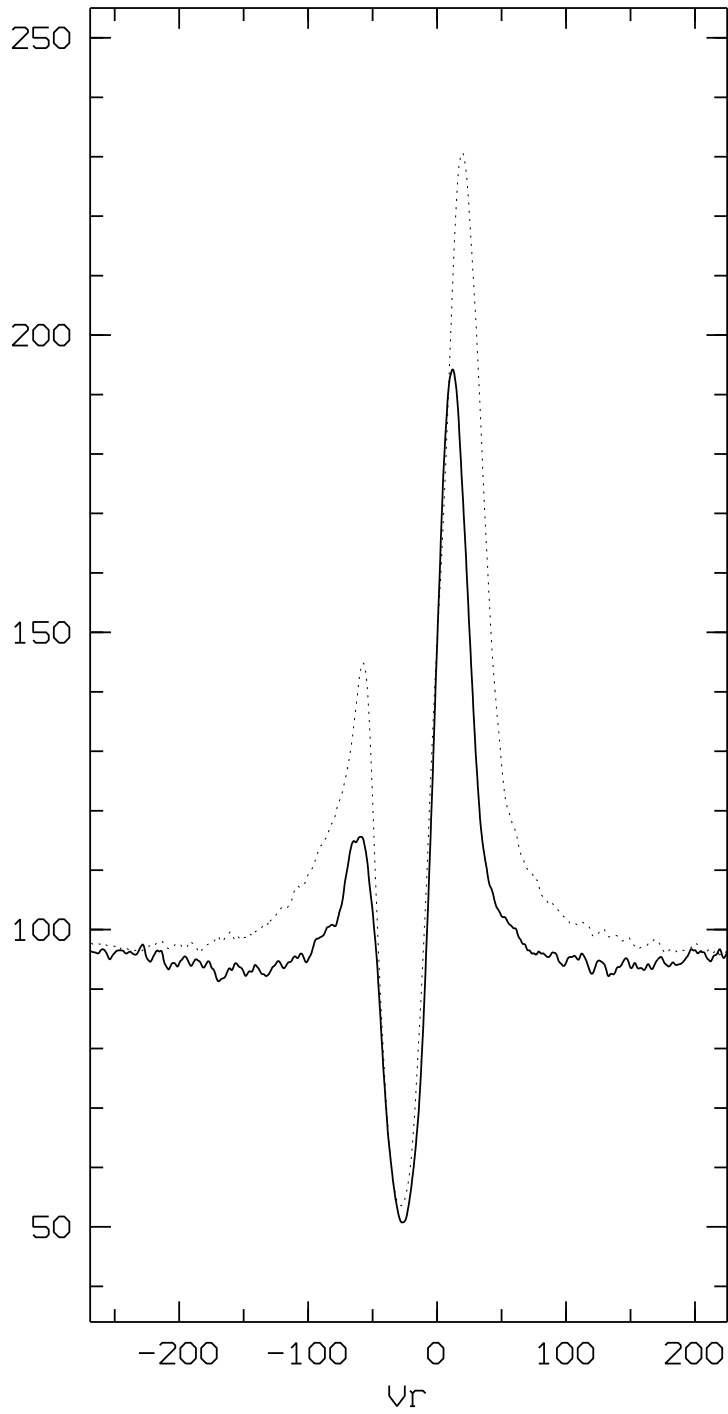


Figure 1. $H\alpha$ line profile in the spectra of BD +48°1220 obtained on March 8, 2004 (solid curve) and January 10, 2004 (dashed curve). The horizontal axis plots radial velocity, the continuum level is specified to be 100.

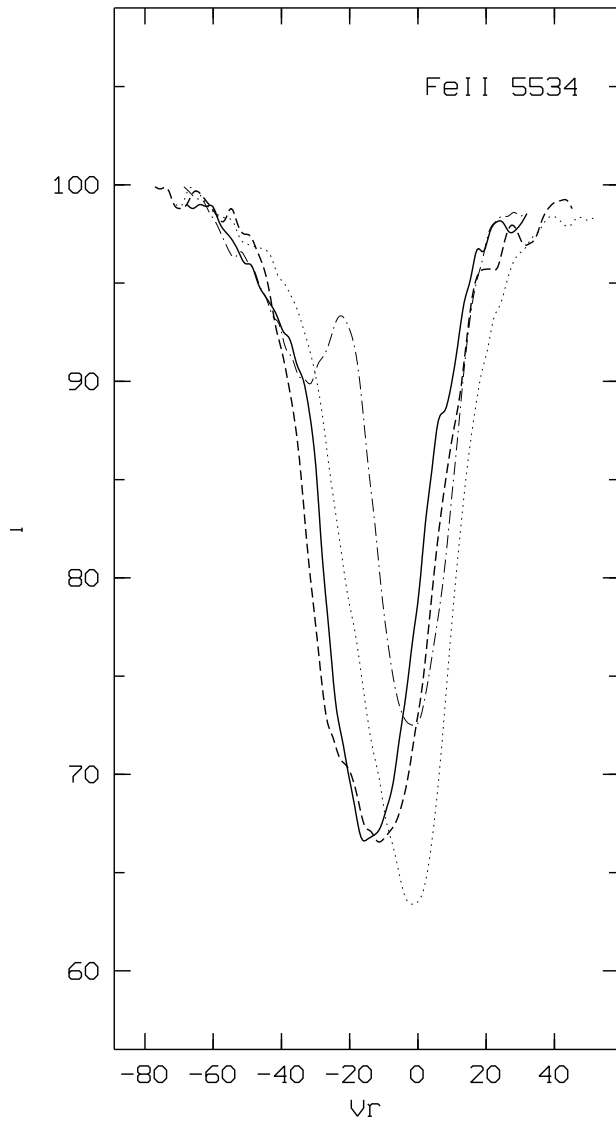


Figure 2. FeII 5534 Å line profile in the spectra of BD +48°1220 obtained on December 2, 2002 (solid curve), September 9, 2003 (dotted curve), January 10, 2004 (dashed curve), and March 8, 2004 (dash-dotted curve). The horizontal axis plots radial velocity, the continuum level is specified to be 100.

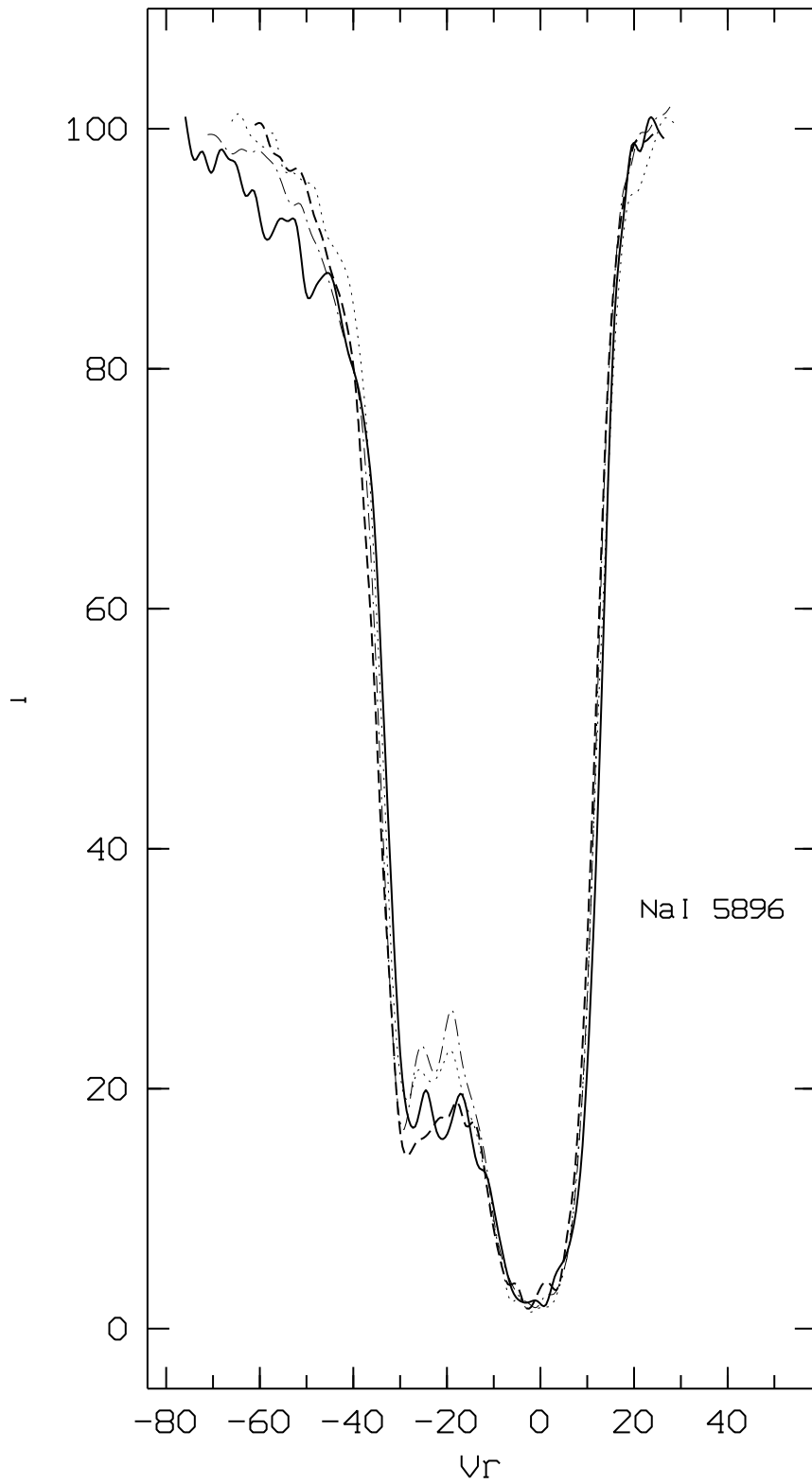


Figure 3. Same as Fig. 2 for the Na D1-line 5896 Å.

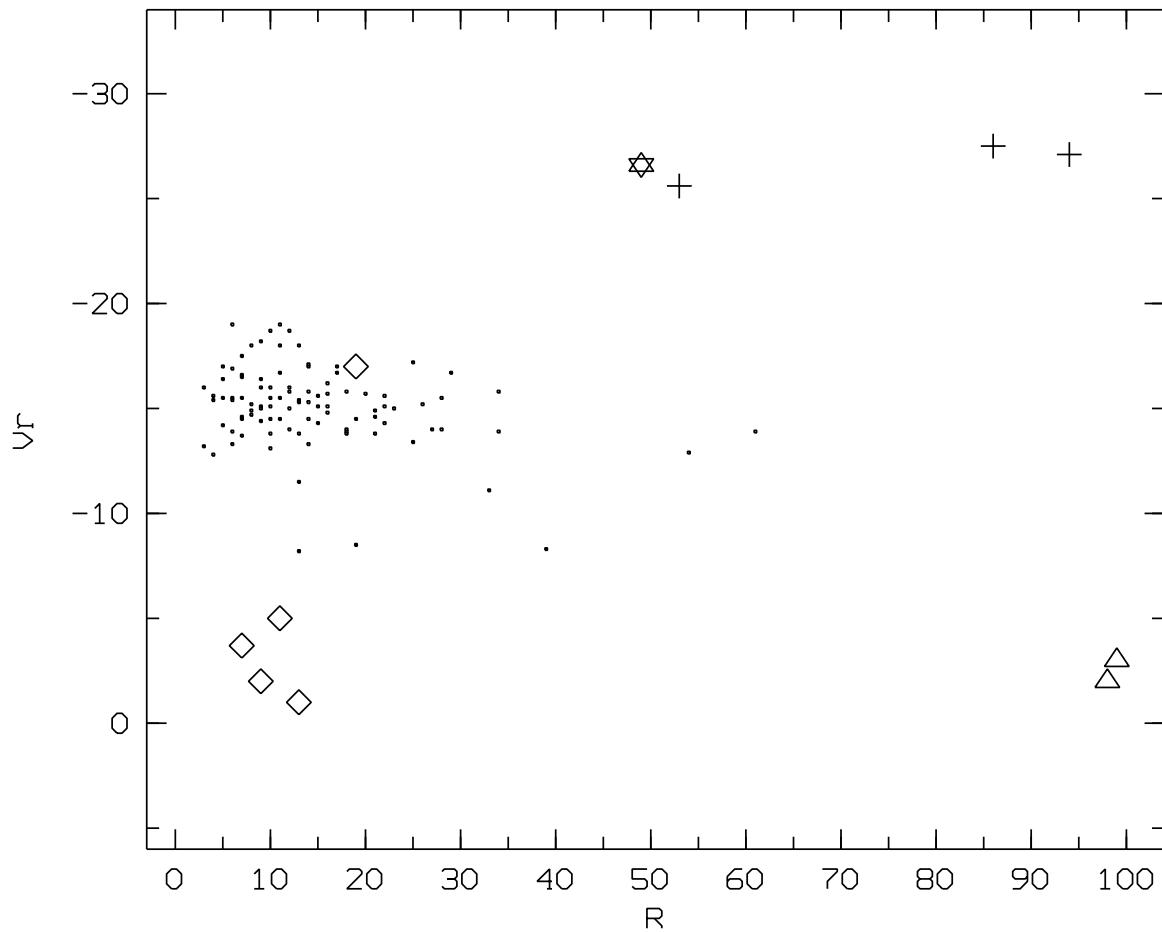


Figure 4. Relation between the radial velocities and central depths derived from lines in the spectrum of BD +48°1220 obtained on January 10, 2004. The asterisk marks the $H\alpha$ line, the crosses the short-wavelength D NaI components and the strong – FeII(49) 5316 Å line, the triangles the D NaI long-wavelength components, and the diamonds – DIBs.

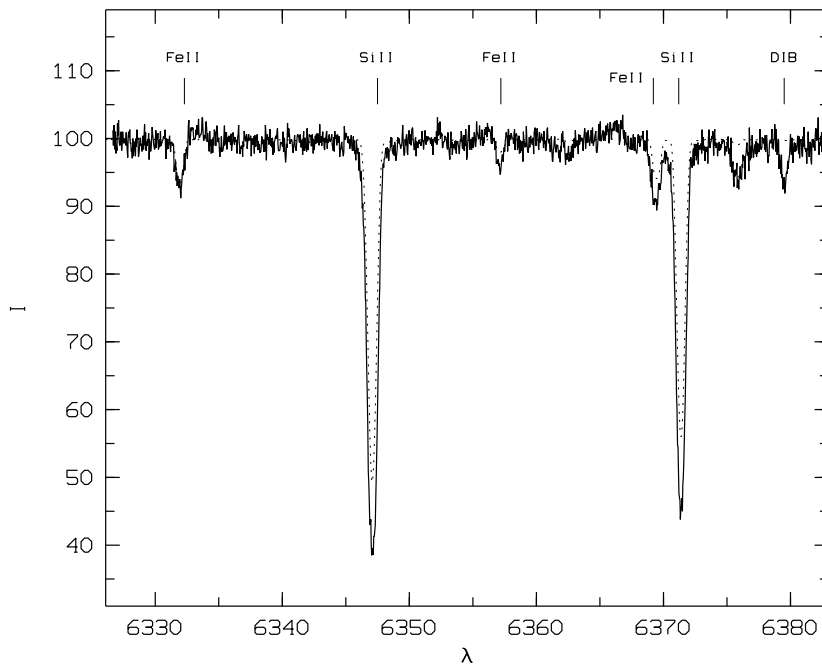


Figure 5. Fragment of the observed spectrum of BD +48°1220 in the vicinity of the SiII 6347, 6371 Å lines (solid curve; the spectrum was obtained on March 8, 2004) together with the theoretical spectrum calculated with the model parameters $T_{eff}=7900$ K, $\log g=0.5$, $\xi_t=6.0$ km/s and the chemical composition from Tabl. 3 (dotted curve).

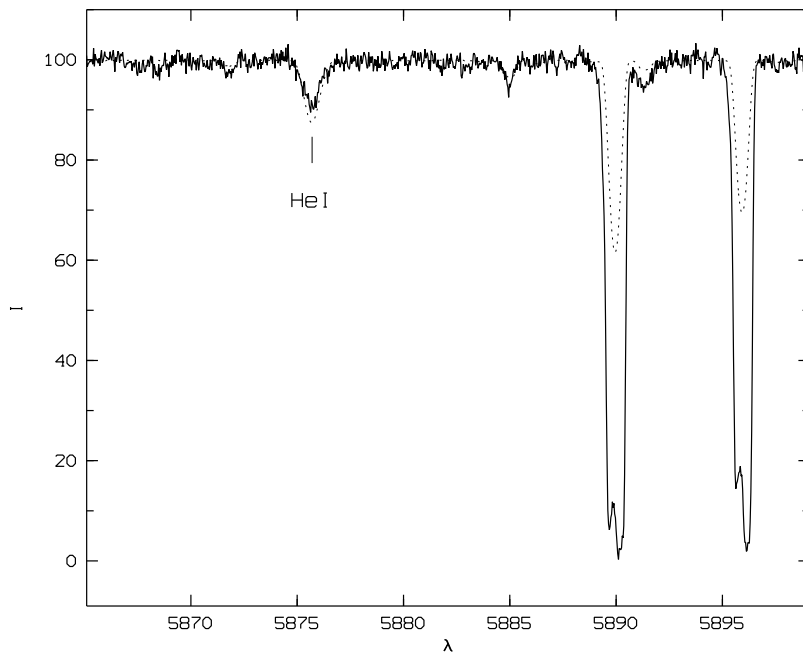


Figure 6. Same as Fig. 5 in the vicinity of the HeI 5876 Å line.

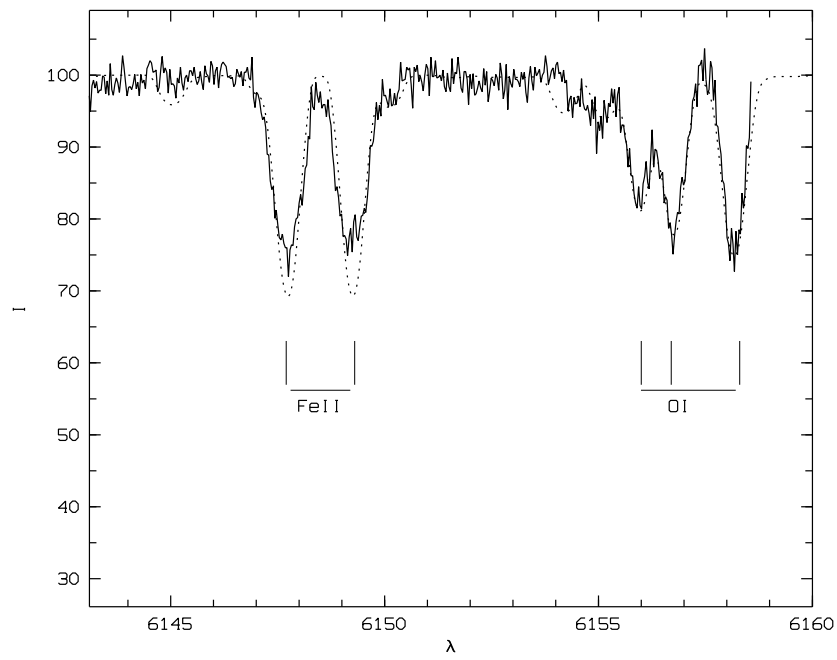


Figure 7. Same as Fig. 5 in the region of the O I 6155 Å lines.

Table 1. Observations of BD +48°1220 with the 6-m telescope

Date	Integration time, s	$\Delta\lambda$ Å	R	S/N
02.12.2002	2×3600	4520–6000	60000	75
09.09.2003	2×3600	4520–6000	60000	100
10.01.2004	2×3600	5280–6760	75000	85
08.03.2004	2×3600	5280–6760	75000	115

Table 2. Diffuse bands in the spectrum of BD +48°1220

λ , Å	W_λ , mÅ
5747	42
5780	227
5797	80
6195	25
6203	64
6270	64
6379	54
6425	13
6613	104
6699	17

Table 3. Average heliocentric radial velocities for line groups and some individual lines, from spectra of BD +48°1220 obtained on different dates. Uncertain values are given by italic

Spectral details	V_{\odot}			
	02.12.02	09.09.03	10.01.04	08.03.04
Absorption cores:				
FeII, CrII, .. ($r \rightarrow 1$)	-14.8	-6.8	-15.3	-8.2
H α			-27	-28
H β	-14.8	-10.6		
Absorbtion line wings at $r=0.90\div 0.95$				
	-14	-9.5	-15.5	-13.0
Maximum extension of short-wavelength wings:				
Fe II(42)	-70	-61	-65	-70
H α			-65	-57
Emissions:				
Fe II(40, 46)				-18
H α			-15	-13
Interstellar lines and bands:				
NaD	-25, -3	-26, -2	-27, -2.5	-28, -2
DIB			-3	-2.5

Table 4. Elemental abundances $\log \varepsilon(X)$ (for $\log \varepsilon(H)=12.0$) in the atmosphere of BD +48°1220. Solar abundances are taken from [23]

Sun		BD +48° 1220, 7900, 0.0, 6.0				
E	$\log \varepsilon(E)$	X	$\log \varepsilon(X)$	σ	n	$[X/Fe]_{\odot}$
He	10.90	HeI	11.84		1	+1.04
Li	3.28	LiI	3.80		1	+0.62
C	8.39	CI	8.38		1	+0.09
O	8.69	OI	9.31	0.17	3	+0.72
Na	6.30	NaI	7.07	0.31	3	+0.87
Mg	7.55	MgI	7.14	0.20	3	-0.31
Si	7.54	SiII	8.20		1	+0.76
			8.25	0.16	3	+0.81
Ca	6.34	CaI	6.04		2	-0.20
Sc	3.07	ScII	2.63	0.28	4	-0.34
Ti	4.92	TiII	4.42	0.19	23	-0.40
V	4.00	VII	3.99	0.03	3	+0.09
Cr	5.65	CrI	5.35	0.12	3	-0.20
		CrII	5.76	0.26	30	+0.21
Mn	5.50	MnI	5.77		1	+0.37
		MnII	5.57		1	+0.17
Fe	7.47	FeI	7.35	0.23	41	-0.07
		FeII	7.44	0.23	68	+0.07
Ni	6.22	NiI	6.86	0.04	3	+0.74
Zn	4.63	ZnI	4.97		2	+0.44
Ba	2.18	BaII	1.24		2	-0.84
Eu	0.52	EuII	-0.61		1	-1.03

Appendix

Table 1. Residual line intensities r in fractions of the continuum and V_{\odot} in the spectra of BD +48° 1220 obtained on various dates. Uncertain values are given by italic

Element (multiplet)	λ , Å	<u>02.12.02</u>		<u>09.09.03</u>		<u>10.01.04</u>		<u>08.03.04</u>	
		r	V_{\odot}	r	V_{\odot}	r	V_{\odot}	r	V_{\odot}
FeI(68)	4528.61	0.73	-17.3	0.76	-11.2				
TiIII(82)	4529.49	0.72	-13	0.71	-6.5				
TiIII(50)	4534.02:	0.37	-	0.35	-				
FeII(37)	4534.16								
CrII(39)	4539.62	0.80	-15.5	0.79	-6.5				
FeII(38)	4541.52	0.49	-13.7	0.49	-5.0				
TiII(60)	4544.01	0.87	-13.0	0.87	-3.5				
TiII(30)	4545.13	0.81	-13.5	0.81	-4.5				
FeII(38)	4549.47	0.35	-	0.31	-				
TiIII(82)	4549.62								
TiII(30)	4552.29	0.90	-13	0.92	-2				
BaI(1)	4554.03	0.85	-12	0.88	-7.6				
CrII(44)	4554.99	0.52	-12.0	0.57	-5.3				
FeII(37)	4555.89	0.40	-16	0.37	-2.0				
CrII(44)	4558.65	0.38	-17	0.36	-1.3				
TiII(50)	4563.76	0.46	-13.1	0.43	-2.6				
VII(56)	4564.58	0.81	-14.5	0.89	-4.5				
CrII(39)	4565.77	0.68	-17	0.71	-9.1				
TiIII(82)	4571.87	0.42	-16	0.38	-1.6				
		(0.93	-60)						
FeII(38)	4576.33	0.51	-14	0.50	-6.1				
FeII	4579.52	0.87	-14	0.85	-4.5				
FeII(26)	4580.05	0.70	-13.3	0.67	-5.9				
FeII(37)	4582.83								
FeII(38)	4583.84	0.40	-22	0.35	-8.4				
CrII(44)	4588.20	0.42	-13.3	0.42	-3.8				
TiIII(50)	4589.94	0.61	-13.1	0.60	-5.0				
-	4593.8	0.85	-	0.88	-				

Element (multiplet)	λ , Å	<u>02.12.02</u>		<u>09.09.03</u>		<u>10.01.04</u>		<u>08.03.04</u>	
		r	V_{\odot}	r	V_{\odot}	r	V_{\odot}	r	V_{\odot}
FeII(38)	4595.68	0.76	–	0.77	–				
FeII(219)	4598.53	0.90	–	0.91	–				
VII(56)	4600.19	0.89	–14	0.90	–7.6				
FeII(43)	4601.36	0.85	–13.4	0.85	–6.5				
CrII(44)	4616.62	0.59	–14.1	0.57	–5.4				
CrII(44)	4618.83	0.47	–14.7	0.45	–5.9				
FeII(38)	4620.51	0.57	–13.3	0.57	–5.2				
SiII	4621.6	0.92	–	0.93	–				
FeII(186)	4625.91	0.86	–16	0.88	–7.6				
FeII(37)	4629.33	0.47	–14.2	0.43	–0.8				
		(0.78	–45)						
FeII(219)	4631.90	0.93	–16	0.95	–				
CrII(44)	4634.07	0.49	–13.0	0.51	–4.7				
		(0.92	–50)						
FeII(186)	4635.31	0.67	–13.9	0.67	–6.9				
–	4638.0	0.86	–	0.86	–				
–	4640.8	0.91	–	0.93	–				
FeII(25)	4648.93	0.83	–15	0.86	–7.3				
FeII(43)	4656.97	0.61	–11	0.60	–3.5				
–	4660.5	0.94	–	0.96	–				
TiII(38)	4662.76	0.90	–	0.90	–				
FeII(44)	4663.70	0.71	–13.4	0.73	–7.3				
–	4665.6	0.93	–	0.91	–				
FeII(37)	4666.75	0.58	–13.4	0.57	–6.7				
FeII(25)	4670.19	0.69	–11.4	0.68	–4.8				
FeI(820)	4673.16	0.93	–	0.94	–				
–	4679.0	0.92	–	0.92	–				
CrII(177)	4697.62	0.92	–13	0.93	–				
MgI(11)	4702.99	0.78	–16.0	0.80	–9.5				
FeI(554)	4707.28	0.95	–11	0.96	–9.5				
TiII(49)	4708.66	0.84	–14.8	0.86	–6.6				
FeII(26)	4713.18	0.91	–15	0.91	–8.2				
NiI(98)	4714.42	0.95	–14	0.94	–9.7				

Element (multiplet)	λ , Å	<u>02.12.02</u>		<u>09.09.03</u>		<u>10.01.04</u>		<u>08.03.04</u>	
		r	V_{\odot}	r	V_{\odot}	r	V_{\odot}	r	V_{\odot}
FeII(54)	4720.13	0.93	-13	0.92	-5				
-	4723.2	0.93	-	0.91	-				
DIB	4726.27	0.97	-	0.98	-				
-	4728.8	0.92	-	0.93	-				
-	4730.3	0.94	-	0.92	-				
FeII(43)	4731.47	0.54	-14.7	0.57	-6.3				
CI	4734.26	0.97	-	0.97	-				
FeI(554)	4736.78	0.91	-11	0.91	-2				
MnII(5)	4738.29	0.90	-14.2	0.90	-8				
MgII(18)	4739.59	0.86	-12.5	0.86	-4.5				
MnII(5)	4755.72	0.82	-14.5	0.84	-5.8				
CI(6)	4762.31	0.87	-	0.84	-				
CI(6)	4762.54								
TiII(17)	4762.78								
NiI(146)	4763.93	0.86	-16.1	0.84	-8.0				
TiII(48)	4764.53	0.84	-5	0.81	2				
CI(6)	4770.03	0.95	-	0.94	-				
CI(6)	4771.75	0.84	-16.8	0.85	-8.6				
FeI(38)	4772.82	0.93	-	0.96	-				
-	4773.8	0.96	-	0.94	-				
CI(6)	4775.91	0.92	-14.2	0.93	-9				
TiII(92)	4779.98	0.66	-14.0	0.69	-5.9				
TiII(17)	4798.53	0.87	-14	0.88	-5.6				
TiII(92)	4805.09	0.61	-13.0	0.61	-5.5				
-	4806.8	0.95	-	0.94	-				
FeII(169)	4810.73	0.91	-19	0.96	-				
CrII(30)	4812.34	0.71	-15.6	0.73	-6.6				
-	4815.6	0.93	-	0.95	-				
-	4820.8	0.94	-	0.96	-				
CrII(30)	4824.14	0.47	-13.6	0.45	-3.2				
FeII(30)	4825.73	0.91	-16.1	0.92	-4				
FeII	4826.68	0.91	-14	0.93	-7.1				
NiI(111)	4831.18	0.91	-16	0.92	-10.6				

Element (multiplet)	λ , Å	<u>02.12.02</u>		<u>09.09.03</u>		<u>10.01.04</u>		<u>08.03.04</u>	
		r	V_{\odot}	r	V_{\odot}	r	V_{\odot}	r	V_{\odot}
FeII(30)	4833.19	0.89	-15.7	0.90	-6.9				
CrII(30)	4836.24	0.71	-14.2	0.68	-7.2				
FeII(30)	4840.00	0.92	-17.5	0.90	-10				
CrII(30)	4848.25	0.52	-12.8	0.50	-4.0				
-	4849.2	0.92	-	0.94	-				
MgII(25)	4851.08	0.88	-15.6	0.89	-10.0				
-	4855.00	<i>0.8</i>	-	<i>0.8</i>	-				
CrII(30)	4856.19	0.70	-15.0	0.70	-8.7				
H β	4861.33	0.30	-14.8	0.29	-10.6				
CrII(30)	4864.32	0.50	-14.0	0.52	-4.1				
TiII(29)	4865.62	<i>0.8</i>	<i>-14</i>	<i>0.85</i>	<i>-8.5</i>				
FeII(30)	4868.82	<i>0.93</i>	-	0.96	-				
FeI(318)	4871.32	0.73	-16.2	0.75	-7.7				
FeI(318)	4872.14	0.88	-12.5	0.88	-8.2				
TiII(114)	4874.01	0.75	-14.2	0.78	-6.0				
CrII(30)	4876.40	0.50	-11.9	0.51	-4.3				
FeI(318)	4878.21	0.93	-12.7	0.93	-8.0				
VII(209)	4883.45	<i>0.93</i>	-	0.91	-				
YII(22)	4883.68	<i>0.97</i>	-	0.93	-				
CrII(30)	4884.60	0.74	-14.0	0.74	-5.5				
FeI(318)	4890.75	0.82	-15.0	0.83	-7.4				
FeI(318)	4891.49	0.78	-14.0	0.82	-7.1				
FeII(36)	4893.81	0.85	-14.3	0.96	-6.8				
YII(22)	4900.12	0.93	<i>-12</i>	0.95	<i>-8:</i>				
CrII(190)	4901.65	0.90	<i>-17.8</i>	0.90	-9.6				
FeI(318)	4903.31	0.93	<i>-13.1</i>	0.95	-5.6				
FeII	4908.15	0.92	<i>-13.7</i>	0.93	-8.3				
TiII(114)	4911.19	0.71	-13.7	0.71	-5.7				
-	4912.4	0.91	-	0.91	-				
FeII	4913.30	0.90	-	0.89	-				
FeI(318)	4918.99	0.84	-16.6	0.85	<i>-8.1</i>				
FeI(318)	4920.50	0.74	-15.3	0.74	-9.0				
HeI(48)?	4921.94	0.94	-12.6	0.94	<i>-5.2</i>				

Element (multiplet)	λ , Å	<u>02.12.02</u>		<u>09.09.03</u>		<u>10.01.04</u>		<u>08.03.04</u>	
		r	V_{\odot}	r	V_{\odot}	r	V_{\odot}	r	V_{\odot}
FeII(42)	4923.92	0.36	-25	0.45	-16				
		0.47	5	0.40	2				
		(0.6	-50)						
Cl(13)	4932.05	0.90	-15.3	0.91	-7.6				
BaII(1)	4934.07	0.89	-14.7	0.90	-6.8				
FeI(318)	4938.81	0.93	-	0.95	-5				
FeII	4948.10	0.92	-14.4	0.93	-7				
FeII	4948.80	0.91	-15.5	0.92	-8				
-	4950.3	0.97	-	0.97	-				
FeII	4951.58	0.86	-16.1	0.87	-9.4				
CrII	4952.78	0.92	-15.9	0.92	-10.5				
FeII(168)	4953.98	0.92	-15.4	0.91	-9.7				
FeI(318)	4957.29								
FeI(318)	4957.58	0.69	-16.9	0.69	-10.9				
-	4958.8	0.97	-	0.97	-				
-	4966.1	0.97	-	0.96	-				
OI(14)	4967.38	0.97	-	0.97	-				
OI(14)	4967.88	0.90	-14.7	0.91	-7.0				
OI(14)	4968.79	0.90	-15.3	0.90	-7.5				
-	4971.3	0.94	-	0.96	-				
FeII	4977.03:	0.88	-15.2	0.89	-9.6				
-	4982.6	0.95	-	0.93	-				
-	4983.8	0.94	-	0.93	-				
FeII	4984.49	0.89	-14.9	0.90	-10.5				
FeII	4990.50	0.85	-14.9	0.87	-8.0				
FeII(25)	4991.11	0.86	-	0.87	-				
-	4992.0	0.94	-	0.94	-				
FeII(36)	4993.35	0.72	-13.5	0.72	-4.9				
FeII	4999.16	0.93	-15	0.94	-7.0				
FeII(25)	5000.73	0.85	-16.0	0.91	-7.3				
CaII(15)	5001.47	0.87	-	-	-				
FeII	5001.92	0.69	-14.1	0.72	-8.2				
FeII	5004.20	0.78	-16.2	0.82	-10.7				
TiII(71)	5005.17	0.96	-	0.96	-				

Element (multiplet)	λ , Å	<u>02.12.02</u>		<u>09.09.03</u>		<u>10.01.04</u>		<u>08.03.04</u>	
		r	V_{\odot}	r	V_{\odot}	r	V_{\odot}	r	V_{\odot}
FeI(984)	5005.71								
FeI(318)	5006.12	0.90	–	0.90	–9				
FeII	5006.84	–	–	0.93	–6				
FeII	5007.45	–	–	0.91	–				
FeII	5007.74	0.91	–	0.91	–				
–	5009.0	0.94	–	0.96	–				
–	5009.5	0.94	–	0.94	–				
TiII(113)	5010.21	0.89	–16.5	0.90	–8.7				
FeI(16)	5012.07	0.96	–	0.95	–8.9				
TiII(71)	5013.69	0.88	–14.5	0.87	–6.9				
FeI(965)	5014.95	0.94	–	0.94	–13.0				
HeI(4)	5015.68								
FeII	5015.75	0.90	–13.8	0.90	–8.5				
FeII(42)	5018.44	0.31	–27.5	0.45	–19				
		0.44	6.2	0.42	2.3				
		(0.57	–54)	(0.79	–47)				
FeII(168)	5019.46	0.84	–16.7	0.86	–7.4				
TiI(38)	5020.02	0.78	–16.8	0.79	–9.7				
OI(13)	5020.22								
FeII	5021.59	0.88	–18.4	0.92	–9.0				
FeII	5022.42	0.87	–	0.89	–				
FeII	5022.79								
CI	5023.85	0.96	–	0.96	–8.5				
–	5024.7	0.95	–	0.94	–				
FeII	5026.80	0.91	–	0.90	–9				
FeI	5027.13								
FeII	5029.10	0.95	–	0.93	–				
FeII	5030.64	0.80	–	0.81	–				
ScII(23)	5031.01	0.83	–	0.84	–				
–	5032.0	0.96	–	0.96	–				
FeII	5032.71	0.88	–16.7	0.88	–12.8				
FeII	5035.71	0.76	–15.7	0.79	–10.5				
FeII(36)	5036.94	0.89	–18.5	0.91	–9.8				
CI(4)	5039.07	0.95	–14.8	0.94	–8.8				
SiII(5)	5041.03	0.61	–15.1	0.62	–7.8				
CI(4)	5041.48	0.92	–	0.92	–				

Element (multiplet)	λ , Å	<u>02.12.02</u>		<u>09.09.03</u>		<u>10.01.04</u>	<u>08.03.04</u>		
		r	V_{\odot}	r	V_{\odot}	r	V_{\odot}	r	V_{\odot}
FeI(66)	5098.70	0.94	-17	0.92	-9				
FeII	5100.74	0.70	-15.2	0.67	-8.6				
FeII	5106.11	0.94	-15	0.93	-9				
FeI(16)	5107.45	0.96	-	0.94	-				
FeI(36)	5107.64								
FeII	5112.99	0.95	-14	0.96	-9				
FeII	5115.06	0.95	-	0.96	-7				
NiI(177)	5115.39								
FeII	5117.03	0.92	-14.0	0.93	-7.8				
FeII	5119.34	0.97	-	0.96	-				
FeII(35)	5120.34	0.84	-13.7	0.84	-7.7				
FeII	5123.19	0.94	-	0.94	-4.2				
YII(21)	5123.22								
FeI(1090)	5125.12	0.95	-	0.96	-5.6				
NiI(160)	5125.23								
FeII(167)	5127.86	0.83	-14.7	0.86	-8.2				
TiII(86)	5129.16	0.76	-14.7	0.75	-5.9				
FeI(66)	5131.47	0.96	-15.7	0.97	-				
FeII(35)	5132.66	0.81	-15.2	0.82	-5.9				
FeI(1092)	5133.68	0.91	-14.0	0.91	-7.0				
-	5134.2	0.95	-	0.95	-				
FeII(35)	5136.80	0.85	-13.3	0.85	-6.0				
NiI(48)	5137.08								
FeI(1090)	5137.38								
FeI(383)	5139.26								
FeI(383)	5139.46	0.87	-	0.87	-				
-	5141.4	0.95	-	0.97	-				
FeI(1092)	5142.53	0.93	-	0.92	-9.0				
FeI(16)	5142.92	0.95	-	0.96	-				
FeII	5143.89	0.91	-13.3	0.93	-				
FeII	5144.36	0.85	-14.6	0.88	-7.1				
FeII	5145.78								
FeII(35)	5146.12	0.79	-	0.78	-				
FeI(1090)	5148.04	0.98	-	0.96	-				
FeI(1095)	5148.23	0.96	-	0.95	-				
FeII	5148.94	0.92	-	0.93	-				

Element (multiplet)	λ , Å	<u>02.12.02</u>		<u>09.09.03</u>		<u>10.01.04</u>		<u>08.03.04</u>	
		r	V_{\odot}	r	V_{\odot}	r	V_{\odot}	r	V_{\odot}
FeI(383)	5232.93	0.77	–	0.76	–				
FeII(49)	5234.62	0.53	–17.8	0.49	0.0				
CrII(43)	5237.32	0.59	–13.6	0.59	–3.3				
FeII	5237.95								
ScII(26)	5239.82	0.88	–14.5	0.89	–7.3				
–	5241.1	0.93	–	0.94	–				
FeII	5243.18								
CrII(38)	5243.50	0.91	–	0.92	–				
CrII(23)	5246.77	0.85	–14.7	0.85	–5.0				
FeII	5247.95	0.83	–14.8	0.86	–8.9				
CrII(23)	5249.43	0.88	–15.4	0.87	–9.4				
FeII	5251.24	0.82	–15.6	0.83	–9.5				
FeI(553)	5253.46								
FeII	5253.64	0.90	–	0.91	–				
FeII(49)	5254.93	0.67	–15.0	0.69	–5.0				
FeII(41)	5256.93	0.81	–	0.80	–				
FeII	5257.11								
FeII	5257.90	0.95	–	0.95	–				
FeII	5258.12								
FeII	5258.41	0.98	–	0.98	–				
FeII	5260.26	0.70	–15.2	0.73	–8.1				
CaI(22)	5261.70	0.97	–	0.97	–				
CaI(22)	5262.24								
FeII	5262.31	0.88	–	0.87	–				
FeI(553)	5263.31	0.96	–	0.96	–				
FeII	5264.18	0.75	–	0.78	–				
FeII(48)	5264.81	0.66	–16.2	0.65	–5.3				
FeI(383)	5266.56	0.90	–14.5	0.92	–				
TiII(103)	5268.62	0.91	–	0.92	–8				
FeI(15)	5269.54	0.80	–14	0.80	–6.8				
CaI(22)	5270.28								
FeI(37)	5270.36	0.88	–	0.89	–10				
FeII	5272.39	0.82	–14.6	0.80	–6.5				
CrII(43)	5274.98	0.63	–11.8	0.59	–4.4				
FeII(49)	5276.00	0.57	–17.2	0.43	0.2				

Element (multiplet)	λ , Å	02.12.02		09.09.03		10.01.04		08.03.04	
		r	V_{\odot}	r	V_{\odot}	r	V_{\odot}	r	V_{\odot}
FeII(225)	5278.20	0.95	–	0.97	–6.6				
FeII(184)	5278.94	0.90	–14.7	0.92	–8.9				
CrII(43)	5279.88	0.71	–8.9	0.71	–3.0				
–	5281.3	0.97	–	0.98	–				
FeI(383)	5281.80	0.94	–	0.97	–				
FeII(41)	5284.10	0.65	–14.6	0.64	–3.4				
–	5285.2	0.97	–	0.96	–				
FeII	5291.67	0.84	–17.3	0.85	–9.5				
–	5294.3	0.97	–	0.98	–				
–	5295.4	0.96	–	0.96	–				
–	5297.1	0.95	–	0.95	–				
FeII	5298.84	0.92	–	0.93	–				
MnII(11)	5299.28	0.92	–	0.92	–6				
–	5299.9	0.97	–	0.97	–				
CrI(18)	5300.75	0.98	–	0.97	–				
FeI(553)	5302.30	0.87	–9.5	0.87	–3.8	0.87	–11.5	0.86	0.0
FeII(225)	5303.39	0.94	–16.7	0.94	–8.6	0.87	–8.2	0.95	–
FeII(184)	5304.27	0.97	–	0.96	–11.3	0.96	–15.4	0.97	–
CrII(24)	5305.86	0.76	–	0.73	–	0.81	–	0.75	–1.9
FeII	5306.18								
FeI(36)	5307.36	0.95	–	0.94	–	0.95	–	0.91	–11.9
CrII(43)	5308.42	0.76	–15.0	0.77	–5.4	0.79	–13.8	0.77	–4.4
CrII(43)	5310.69	0.83	–15.1	0.85	–6.7	0.86	–17.0	0.83	–4.0
CrII(43)	5313.58	0.70	–14.3	0.70	–5.2	–	–	–	–
FeII(49)	5316.65:	0.51	–23	0.44	1.7	0.47	–25.6	0.40	–40
FeII(48)		0.55	–1			0.54	–7.5	0.59	0
YII(20)	5320.78	0.98	–	0.96	–	0.95	–	0.98	–
FeI(112)	5322.04	0.95	–	0.95	–	0.92	–	0.96	–
FeI(553)	5324.17	0.86	–13.3	0.86	–6.5	0.84	–15.7	0.81	–5.0
FeII(49)	5325.56	0.70	–13.7	0.66	–4.3	0.71	–16.7	0.70	–2.9
FeI(15)	5328.03	0.82	–13.8	0.84	–4.4	0.85	–14.3	0.79	–4.1
OI(12)	5329.10	0.88	–14.0	0.89	–6.2	0.88	–	0.89	–4.7
OI(12)	5329.69	0.84	–15.6	0.86	–7.1	0.84	–14.8	0.88	–5.5

Element (multiplet)	λ , Å	02.12.02		09.09.03		10.01.04		08.03.04	
		r	V_{\odot}	r	V_{\odot}	r	V_{\odot}	r	V_{\odot}
OI(12)	5330.74	0.83	-15.1	0.83	-8.8	0.82	-14.0	0.85	-4.9
CrII(43)	5334.87	0.71	-14.2	0.71	-6.0	0.72	-14	0.72	-3.4
FeII(48)	5337.73	0.71	-14.5	0.73	-6.1	0.72	-15.5	0.77	-2.2
FeII	5339.59	0.81	-14.6	0.83	-9.1	0.82	-	0.82	-
FeI(553)	5339.93								
FeI(37)	5341.03	0.93	-15.2	0.95	-6.5	0.95	-	0.91	-
CrI(18)	5345.80								
CrII(24)	5346.08	0.89	-	0.89	-6	0.90	-	0.87	-4.4
CrII(23)	5346.54	0.90	-	0.89	-	0.90	-	0.90	-
FeII	5358.87	0.95	-	0.95	-7.5	0.96	-	0.97	-
FeII(48)	5362.86	0.62	-17.0	0.58	-0.6	0.61	-8.3	0.84	-30
								0.69	-2.3
FeI(1146)	5364.87	0.95	-14.7	0.94	-7.1	0.94	-15.4	0.92	-5.2
FeII	5366.21	0.96	-14.7	0.95	-10.2	0.96	-15.6	0.97	-5
FeI(1146)	5367.47	0.92	-16.0	0.92	-8.1	0.93	-16.6	0.91	-6.7
FeI(15)	5371.49	0.87	-16.8	0.89	-9.1	0.88	-18.7	0.85	-7.1
FeII	5375.84	0.92	-14.0	0.94	-	0.94	-16.9	0.95	-3
CI(11)	5380.32	0.91	-14.8	0.92	-8.0	0.94	-	0.91	-3.6
TiII(69)	5381.03	0.87	-16.0	0.86	-6.3	0.89	-19	0.84	-5.4
FeI(1146)	5383.37	0.86	-15.0	0.86	-8.1	0.86	-15.8	0.85	-6.1
FeII	5387.07	0.83	-15.2	0.85	-9.0	0.86	-17.1	0.87	-5.2
FeI(553)	5393.17	0.95	-	0.95	-8.7	0.95	-	0.94	-8
FeII	5393.8:	0.93	-	0.95	-	0.93	-	0.96	-
FeII	5395.86	0.85	-16.5	0.86	-9.4	0.89	-14.5	0.87	-5.1
FeI(15)	5397.12	0.90	-	0.93	-8.9	0.89	-18	0.89	-8.8
-	5401.6	0.83	-	0.85	-	0.85	-	0.86	-
FeII	5402.06	0.83	-16.7	0.87	-	0.85	-	0.89	-6.5
FeI(1145)	5404.12	0.87	-13.7	0.88	-6.7	-	-	-	-
FeII	5405.10	0.93	-	0.93	-8.7	0.93	-	0.92	-
FeI(15)	5405.77	0.90	-15.8	0.90	-8.4	0.90	-18.7	0.87	-8.3
CrII(23)	5407.62	0.82	-15.3	0.83	-6.0	0.84	-15.1	0.83	-5.2
FeII(48)	5414.07	0.75	-13.9	0.77	-6.5	0.79	-14.9	0.94	-27
								0.77	-3.1
TiII(69)	5418.77	0.91	-15.7	0.88	-4.9	0.91	-16.4	0.88	-5.3

Element (multiplet)	λ , Å	02.12.02		09.09.03		10.01.04		08.03.04	
		r	V_{\odot}	r	V_{\odot}	r	V_{\odot}	r	V_{\odot}
CrII(23)	5420.93	0.86	-13.2	0.85	-5.5	0.87	-13.8	0.85	-3.9
FeI(1146)	5424.07	0.84	-15.7	0.86	-7.5	0.88	-15.0	0.82	-5.8
FeII(49)	5425.25	0.70	-15.0	0.70	-4.7	0.73	-14.0	0.90	-34
								0.72	-2.9
FeII	5427.80	0.87	-14.8	0.88	-7.7	0.89	-15.5	0.91	-1.9
FeII	5432.98	0.74	-15.6	0.76	-7.6	0.75	-17.2	0.93	-32.5
								0.76	-5.0
FeI915)	5434.52	0.96	-	0.96	-6:	0.97	-	0.93	-
OI(11)	5435.78	0.94	-	0.95	-9.9	0.95	-16.4	0.93	-3.0
OI(11)	5436.86	0.91	-17.3	0.94	-6	0.94	-	0.93	-5.0
FeII	5445.80	0.94	-	0.93	-9.8	0.93	-	0.93	-4.0
FeII	5457.72	0.95	-	0.96	-10.5	0.94	-	0.95	-
FeII	5465.93	0.84	-12.9	0.87	-8	0.87	-	0.86	-3.6
FeII	5466.92	0.88	-16.9	0.88	-10	0.88	-16	0.89	-5.0
CrII(50)	5478.37	0.79	-14.6	0.77	-6.5	0.79	-14.6	0.78	-3.9
FeII	5482.31	0.86	-14.5	0.87	-8.8	0.88	-15.8	0.88	-4.5
FeII	5487.63	0.85	-17.2	0.86	-9.5	0.86	-15.3	0.85	-5.9
CrII(50)	5502.08	0.81	-13.8	0.80	-6.0	0.82	-13.8	0.80	-3.3
CrII(50)	5503.22	0.80	-13.9	0.82	-5.8	0.83	-17	0.83	-3.5
FeII	5506.20	0.79	-14.5	0.78	-9.2	0.78	-14.3	0.79	-2.5
CrII(50)	5508.62	0.85	-15.2	0.83	-4.1	0.85	-15.1	0.83	-4.3
CrII(23)	5510.71								
FeII	5510.78	0.86	-	0.82	-8	0.83	-16.7	0.83	-5.7
FeII(56)	5525.11	0.86	-13.5	0.88	-5.0	0.89	-16.7	0.86	-3.6
ScII(31)	5526.81	0.84	-15.2	0.81	-5.1	0.85	-15.6	0.78	-6.8
MgI(9)	5528.40	0.81	-15.0	0.83	-8.4	0.84	-16.2	0.80	-6.5
FeII(224)	5529.93	0.91	-14.8	0.92	-7.5	0.92	-14.9	0.92	-2.2
FeII	5532.09	0.96	-15.2	0.94	-9.1	0.95	-17	0.96	-4.8
FeII(55)	5534.84	0.68	-13.4	0.63	-1.7	0.67	-11.1	0.91	-33
								0.72	-1.8
OI(24)	5554.9:	0.93	-	0.93	-	0.94	-	0.94	-
FeII	5567.84	0.93	-15.8	0.92	-8.2	0.94	-19:	0.97	-2.9
FeI(686)	5572.84	0.90	-14.7	0.90	-5.9	0.92	-15.2	0.91	-5.7

Element (multiplet)	λ , Å	<u>02.12.02</u>		<u>09.09.03</u>		<u>10.01.04</u>		<u>08.03.04</u>	
		r	V_{\odot}	r	V_{\odot}	r	V_{\odot}	r	V_{\odot}
FeI(686)	5586.76	0.89	–	0.88	–4.5	0.87	–	0.85	–6.5
FeII	5587.08								
FeII	5588.22	0.90	–14.7	0.91	–10	0.90	–13.8	–	–
FeI(686)	5615.65	0.87	–15.7	0.87	–8.0	0.88	–14.0	0.84	–5.4
CrII(189)	5620.63	0.96	–	0.95	–7.1	0.95	–	0.95	–3
FeII(57)	5627.49	0.90	–14.9	0.92	–7.1	0.90	–15.1	0.89	–2.1
FeII	5645.40	0.90	–	0.90	–9.5	0.92	–	0.92	–4.3
FeII	5648.90	0.94	–18.5	0.95	–8.3	0.93	–	0.96	–
ScII(29)	5669.03	0.94	–	0.93	–8.8	0.93	–17.5	0.92	–10
NaI(6)	5688.21	0.94	–15	0.90	–7.7	0.93	–14.5	0.93	–6.5
FeII(164)	5747.90	0.93	–16.6	0.93	–7.4	0.93	–	0.94	–5.2
DIB	5780.37	0.84	–	0.80	–	0.81	–17	0.82	–13
DIB	5796.96	0.90	6	0.91	2	0.91	–2	0.89	0
FeII	5811.63	0.95	–13	0.96	–7.0	0.97	–	0.97	–
FeII(164)	5823.15	0.94	–15.3	0.94	–6.9	0.95	–14.2	0.93	–4.0
FeII(182)	5835.49	0.94	–12.8	0.94	–8.5	0.94	–13.9	0.95	–1.4
HeI(11)	5875.72	0.90	–15	0.91	–11.0	0.90	–16	0.93	–8.8
NaI(1)	5889.95	0.08	–26	0.09	–25.9	0.06	–27.1	0.10	–28
		0.01	–4.5	0.02	–2.7	0.01	–3	0.02	–3.5
NaI(1)	5895.92	0.17	–24	0.19	–26	0.14	–27.5	0.17	–29
		0.02	–2	0.02	–1.4	0.02	–2	0.02	–1.1
SiII(4)	5957.56	0.80	–15.6	0.79	–9.6	0.81	–14.5	0.81	–6.1
FeII	5961.75	0.84	–17	0.86	–11.8	0.87	–18.0	0.88	–6.9
SiII(4)	5978.93	0.73	–15.5	0.75	–10.5	0.74	–15.2	0.75	–4.5
FeII(46)	5991.37	0.86	–15.3	0.82	–3.0	0.86	–14.5	0.85	–0.1
FeI(1178)	6024.06					0.94	–13.3	0.93	–7.2
CrII(105)	6053.46					0.93	–14.6	0.93	–3.1
FeII(20)	6103.54					0.92	–18.0	0.93	–3.8
FeII(46)	6113.33					0.90	–14.5	0.91	–3.3
FeII(74)	6147.74					0.75	–13.4	0.91	–32
								0.78	–2.9
FeII(74)	6149.25					0.78	–15.1	0.91	–30.5
								0.78	–2.1

Element (multiplet)	λ , Å	02.12.02		09.09.03		10.01.04		08.03.04	
		r	V_{\odot}	r	V_{\odot}	r	V_{\odot}	r	V_{\odot}
OI(10)	6155.98					0.82	-15.8	0.82	-2.8
OI(10)	6156.77					0.78	-15.6	0.76	-3.7
OI(10)	6158.18					0.77	-15.0	0.69	-4.3
FeII	6175.14					0.90	-13.1	0.91	-3.0
CrII(187)	6179.17								
FeII(163)	6179.38					0.93	-16.5	0.92	-3.6
CrII(105)	6195.18					0.97	-13.2	0.98	-
-	6196.2					0.94	-	0.95	-
FeII(162)	6199.19					0.96	-12.8	0.96	-3.2
FeII(74)	6238.39					-	-	0.91	-33
								0.77	-2.6
FeII(74)	6247.55					0.66	-13.9	-	-
FeII	6248.89					0.91	-14.4	-	-
FeII	6269.97					0.91	-16.0	0.91	-4.2
DIB	6283.85					0.87	-1	0.85	-5.5
FeII(200)	6305.29					0.91	-15.1	-	-
FeII	6317.99					0.80	-15.7	0.90	-33
								0.78	-3.0
FeII(199)	6331.95					0.93	-15.5	0.92	-3.0
SiII(2)	6347.10					0.39	-13.9	0.52	-7.7
FeII	6357.17					0.95	-15.5	0.97	-7
FeII(40)	6369.46					0.91	-18.2	0.97	-33
								0.91	-1.6
SiII(2)	6371.36					0.46	-12.9	0.55	-5.0
DIB	6379.29					0.93	-3.7	0.88	-4.1
FeII	6383.72					0.87	-15.3	0.84	-3.5
FeII	6385.46					0.90	-15.5	0.90	-3.7
FeI(816)	6400.01					0.94	-15.5	0.95	-
FeII(74)	6416.92					0.81	-8.5	0.94	-33
								0.84	-2.7
FeII(40)	6532.68					0.86	-13.3	0.96	-36
								0.88	-1.1
CaI(18)	6439.08					0.97	-16.0	0.94	-13.6
FeII	6442.95					0.92	-14.7	0.89	-3.5

Element (multiplet)	λ , Å	02.12.02		09.09.03		10.01.04		08.03.04	
		r	V_{\odot}	r	V_{\odot}	r	V_{\odot}	r	V_{\odot}
FeII(199)	6446.40					0.91	-15.0	0.91	-2.4
FeII(74)	6456.38					0.66	-15.8	0.76	-29
								0.77	3.3
FeII(199)	6482.19					0.87	-15.4	0.87	-1.0
FeII	6506.33					0.93	-13.7	0.95	-0.4
FeII(40)	6516.08					0.85	-	0.97	-36
								0.87	-1.9
FeII	6517.02					-	-	0.92	-3.7
MgII(23)	6545.97					0.82	-13.9	0.84	-3.6
H α	6562.81					0.51	-26.6	0.53	-28
						(em	-15.5		-13)
DIB	6613.56					0.89	-5	0.89	-1.5

Table 2. Atomic parameters of the lines in the spectrum of BD +48°1220 obtained on January 10, 2004, and the corresponding elemental abundances $\log \varepsilon(X)$ (for $\log \varepsilon(H)=12$) in the atmosphere of BD +48°1220 obtained with parameters $T_{eff} = 7900$ K, $\log g=0.5$, $\xi_t = 6.0$.

Element/ λ	EP, ev	$\log gf$	W_{λ}	$\log \varepsilon(X)$
HeI				
5875.62	20.964	0.409	75	0.12
LiI				
6707.76	0.000	-0.009	10	-8.39
CI				
5039.050	7.4828	-2.100	23	-3.77
OI				
6155.966	10.7400	-1.011	117	-2.54
6156.776	10.7400	-0.694	152	-2.61
6158.185	10.7400	-0.409	155	-2.87
NaI				
5682.633	2.102	-0.70	25	-5.46
5688.194	2.104	-1.40	20	-4.86
6160.747	2.104	-1.26	18	-5.04
MgI				
5167.330	2.7100	-0.860	196	-5.07
5183.620	2.7200	-0.160	270	-5.26
5528.405	4.3400	-0.620	79	-4.82
SiII				

Element/ λ	EP, eV	$\log gf$	W_λ	$\log \varepsilon(X)$
4621.418	12.5254	-0.540	35	-3.89
6347.090	8.1200	0.260	561	-3.75
6371.350	8.1200	-0.160	490	-3.51
CaI				
4878.126	2.7090	0.430	25	-6.04
6439.075	2.5200	0.394	14	-6.47
ScII				
5239.813	1.4551	-0.765	42	-9.52
5526.790	1.7680	0.024	90	-9.67
5657.896	1.5070	-0.603	120	-9.06
5669.042	1.5000	-1.200	34	-9.17
TiII				
4529.474	1.5718	-1.650	138	-7.48
4544.028	1.2429	-2.530	39	-7.58
4545.133	1.1305	-2.460	75	-7.40
4552.294	1.1156	-2.890	41	-7.30
4563.761	1.2214	-0.790	324	-7.31
4589.958	1.2369	-1.620	169	-7.59
4708.665	1.2370	-2.370	64	-7.51
4762.776	1.0842	-2.880	50	-7.25
4779.985	2.0480	-1.260	152	-7.44
4798.521	1.0800	-2.670	46	-7.51
4805.085	2.0613	-0.960	192	-7.51
4874.014	3.0950	-0.900	104	-7.30
4911.193	3.1240	-0.650	147	-7.29
5013.677	1.5818	-1.990	54	-7.74
5069.090	3.1236	-1.540	22	-7.48
5129.152	1.8920	-1.300	110	-7.79
5154.070	1.5660	-1.780	124	-7.48
5188.680	1.5818	-1.050	180	-7.89
5211.536	2.5903	-1.356	42	-7.76
5226.543	1.5658	-1.230	189	-7.67
5268.615	2.5977	-1.670	28	-7.63
5381.015	1.5660	-1.970	56	-7.77
5418.751	1.5818	-2.110	46	-7.72
VII				
4564.579	2.2680	-1.393	48	-7.94
4600.166	2.2651	-1.523	34	-7.99
4883.407	3.7957	-0.778	17	-7.95
CrI				
5204.506	0.9414	-0.208	25	-6.94
5206.038	0.9410	0.019	47	-6.86
5208.419	0.9414	0.158	80	-6.72
CrII				
4539.595	4.0424	-2.290	86	-6.16

Element/ λ	EP, ev	$\log gf$	W_λ	$\log \varepsilon(X)$
4558.650	4.0735	-0.449	413	-5.53
4565.740	4.0424	-1.820	107	-6.49
4588.199	4.0710	-0.627	309	-6.26
4616.629	4.0723	-1.361	212	-6.28
4634.070	4.0723	-0.990	250	-6.38
4697.598	5.6699	-1.880	18	-6.24
4812.337	3.8645	-1.960	121	-6.41
4836.229	3.8581	-1.960	134	-6.33
4848.235	3.8645	-1.151	266	-6.24
4876.399	3.8538	-1.460	260	-6.01
4884.607	3.8581	-2.100	96	-6.43
4901.623	6.4871	-0.826	42	-6.33
4952.794	6.2820	-1.436	37	-5.92
5210.865	3.7577	-2.945	48	-6.06
5237.329	4.0730	-1.160	226	-6.43
5249.437	3.7580	-2.489	65	-6.35
5274.964	4.0713	-1.290	240	-6.22
5279.876	4.0735	-2.100	207	-5.62
5305.853	2.5870	-2.357	165	-6.72
5308.408	4.0710	-1.846	140	-6.27
5313.563	4.0740	-1.650	181	-6.23
5407.604	3.8268	-2.152	100	-6.39
5420.922	3.7577	-2.458	75	-6.30
5502.067	4.1680	-1.990	129	-6.12
5503.212	4.1434	-2.306	124	-5.85
5508.606	4.1560	-2.110	110	-6.13
5510.702	3.8268	-2.452	125	-5.93
5620.631	6.4871	-1.145	36	-6.07
6053.466	4.7450	-2.229	62	-5.92
MnI				
4762.367	2.8884	0.425	41	-6.42
MnII				
4755.727	5.3970	-1.242	80	-6.37
FeI				
4707.274	3.2410	-1.080	12	-4.82
4736.773	3.2112	-0.752	41	-4.59
4871.318	2.8654	-0.363	112	-4.64
4878.211	2.8852	-0.888	25	-4.93
4890.755	2.8755	-0.394	64	-4.97
4891.492	2.8512	-0.112	81	-5.14
4903.310	2.8820	-0.926	26	-4.89
4920.503	2.8325	0.068	118	-5.09
4938.813	2.8755	-1.077	28	-4.71
5006.119	2.8325	-0.638	33	-5.10
5012.068	0.8590	-2.642	11	-5.08

Element/ λ	EP, ev	$\log gf$	W_λ	$\log \varepsilon(X)$
5014.942	3.9430	-0.303	17	-4.94
5065.014	4.2563	-0.134	37	-4.52
5074.748	4.2200	-0.200	26	-4.64
5078.972	4.3013	-0.521	16	-4.49
5090.774	4.2560	-0.400	15	-4.67
5098.698	2.1760	-2.026	18	-4.50
5125.117	4.2204	-0.140	19	-4.85
5133.688	4.1780	0.140	32	-4.91
5137.382	4.1780	-0.400	11	-4.87
5139.462	2.9399	-0.509	48	-4.97
5142.542	4.3013	-0.174	21	-4.71
5148.225	4.2563	-0.274	7	-5.15
5162.272	4.1780	0.020	33	-4.79
5171.596	1.4850	-1.793	38	-4.89
5191.455	3.0385	-0.551	42	-4.93
5192.344	2.9981	-0.421	36	-5.17
5202.336	2.1760	-1.838	14	-4.80
5232.940	2.9400	-0.058	142	-4.76
5263.306	3.2660	-0.879	13	-4.99
5266.555	2.9980	-0.386	37	-5.19
5324.179	3.2110	-0.103	65	-5.03
5328.038	0.9146	-1.466	100	-5.13
5371.489	0.9580	-1.645	68	-5.15
5404.112	4.3125	0.218	46	-4.73
5405.775	0.9900	-1.844	45	-5.14
5424.068	4.3200	0.520	61	-4.87
5572.842	3.3970	-0.275	47	-4.90
5615.643	3.3320	0.050	60	-5.14
6024.058	4.5490	-0.120	29	-4.44
6400.001	3.6026	-0.290	15	-5.28
FeII				
4579.527	6.2257	-2.508	40	-4.26
4580.063	2.5827	-3.725	159	-4.67
4582.835	2.8440	-3.090	251	-4.51
4598.494	7.8043	-1.497	46	-4.21
4601.378	2.8910	-4.428	52	-4.48
4620.521	2.8281	-3.240	200	-4.73
4625.893	5.9562	-2.202	65	-4.47
4629.339	2.8067	-2.330	317	-4.77
4631.873	7.8687	-1.873	20	-4.22
4635.316	5.9600	-1.650	161	-4.35
4648.944	2.5827	-4.389	69	-4.59
4656.981	2.8900	-3.610	210	-4.26
4663.708	2.8786	-4.265	106	-4.24
4666.758	2.8300	-3.330	198	-4.66

Element/ λ	EP, ev	$\log gf$	W_λ	$\log \varepsilon(X)$
4670.182	2.5800	-4.060	167	-4.30
4713.193	2.7785	-4.932	36	-4.25
4720.149	3.1973	-4.750	30	-4.22
4731.453	2.8910	-3.000	234	-4.71
4810.745	5.5688	-3.227	19	-4.33
4825.736	2.6349	-4.829	27	-4.59
4833.197	2.6571	-4.780	37	-4.47
4839.998	2.6758	-4.900	33	-4.39
4893.820	2.8281	-4.450	59	-4.45
4953.987	5.5706	-2.757	31	-4.56
4991.126	2.7785	-4.365	60	-4.56
4993.358	2.8067	-3.640	145	-4.70
5000.743	2.7785	-4.540	43	-4.56
5074.053	6.8073	-1.973	34	-4.48
5120.352	2.8281	-4.214	71	-4.59
5127.866	5.5706	-2.535	71	-4.33
5132.669	2.8070	-3.980	84	-4.74
5136.802	2.8440	-4.290	72	-4.49
5197.577	3.2300	-2.100	290	-5.00
5215.844	8.1453	-0.227	79	-4.86
5234.625	3.2210	-2.230	330	-4.57
5254.929	3.2305	-3.227	173	-4.64
5256.938	2.8786	-4.250	90	-4.38
5264.812	3.2300	-3.120	210	-4.53
5272.397	5.9562	-2.030	75	-4.53
5276.002	3.1995	-1.940	320	-4.96
5284.109	2.8910	-2.990	219	-4.86
5326.053	3.2210	-3.120	188	-4.67
5414.073	3.2210	-3.540	140	-4.53
5425.257	3.1990	-3.160	191	-4.63
5432.967	3.2674	-3.629	174	-4.21
5525.125	3.2674	-3.950	65	-4.59
5534.847	3.2450	-2.730	250	-4.66
5627.497	3.3866	-4.130	54	-4.42
5747.884	5.5706	-2.909	55	-4.07
5813.677	5.5706	-2.750	76	-4.04
5823.155	5.5688	-3.070	33	-4.18
5835.492	5.9110	-2.372	36	-4.59
5952.510	5.9562	-2.032	49	-4.73
5991.376	3.1530	-3.540	108	-4.77
6103.496	6.2170	-2.171	71	-4.19
6113.322	3.2210	-4.110	66	-4.45
6147.741	3.8887	-2.721	205	-4.46
6175.146	6.2226	-1.983	81	-4.29
6179.384	5.5688	-2.810	46	-4.25

Element/ λ	EP, ev	$\log gf$	W_λ	$\log \varepsilon(X)$
6248.898	5.5108	-2.696	62	-4.23
6317.983	5.5108	-1.990	155	-4.28
6331.954	6.2170	-1.977	56	-4.51
6369.462	2.8910	-4.160	66	-4.64
6383.722	5.5530	-2.070	93	-4.57
6385.451	5.5527	-2.618	60	-4.29
6416.919	3.8920	-2.650	163	-4.77
6432.680	2.8910	-3.520	119	-4.91
6516.080	2.8910	-3.320	152	-4.92
NiI				
4980.166	3.6060	0.070	63	-5.30
5017.568	3.5390	-0.020	56	-5.33
5476.900	1.8260	-0.890	111	-5.34
ZnI				
4810.528	4.0780	-0.137	24	-7.36
6362.338	5.7960	0.150	6	-7.05
BaII				
4554.029	0.0000	0.170	62	-10.98
6141.710	0.7040	-0.080	20	-10.83
EuII				
6645.064	0.2050	1.380	18	-12.71